Research Article

Visible light-driven superoxide generation by conjugated polymers for organic synthesis

Feili Lai[1,2], Yue Wang[2], Dandan Li[3], Xianshun Sun[1], Juan Peng[2], Xiaodong Zhang[1] (✉), Yupeng Tian[3], and Tianxi Liu[2,4] (✉)

[1] *Hefei National Laboratory for Physical Science at Microscale Collaborative Innovation Center of Chemistry for Energy Materials, University of Science and Technology of China, Hefei 230026, China*

[2] *State Key Laboratory of Molecular Engineering of Polymers, Department of Macromolecular Science, Fudan University, Shanghai 200433, China*

[3] *Department of Chemistry, Anhui University, Hefei 230039, China*

[4] *State Key Laboratory of Modification of Chemical Fibers and Polymer Materials, College of Materials Science and Engineering, Donghua University, Shanghai 201620, China*

ABSTRACT

Benefiting from their unique delocalized electronic structure, conjugated polymer-based semiconductors are widely applied in the fields of organic electronics, sensors, and biomedical applications. However, the photocatalytic properties of conjugated polymers have been seldom studied because of their unsuitable band structures. Herein, we creatively demonstrate that the band structures of conjugated polymers are strongly related to their degree of polymerization (DP), offering an effective strategy for the design of metal-free photocatalysts with tunable light absorption properties. Taking poly(3-hexylthiophene) (PHT) as an example, we show that PHT nanofibers with a suitable DP are a novel visible light-driven photocatalyst, which can readily convert molecular oxygen into superoxide ions. Benefiting from the high selectivity of the generated superoxides, the PHT nanofibers display outstanding activity for the aerobic oxidation of amines into imines with nearly 100% conversion and selectivity. This study offers a new strategy for the design of advanced conjugated polymer-based photocatalysts.

1 Introduction

Light-driven organic synthesis is of great interest for both its environmental and economic values owing to its potential application in the conversion of clean solar energy into chemical energy [1, 2]. Under the controlled photogeneration of reactive oxygen species (ROS) by catalysts, such as hydroxyl radical (·OH), superoxide (O_2^-), and singlet oxygen ($^1O_2$) [3–6], light-driven organic synthesis may achieve both higher

Address correspondence to Xiaodong Zhang, zhxid@ustc.edu.cn; Tianxi Liu, txliu@fudan.edu.cn, txliu@dhu.edu.cn

conversions and selectivity rates than traditional strategies. With this aim, great efforts have been carried out in the search for efficient catalysts for light-driven organic synthesis. Although metal oxides and metal sulfides have been regarded as promising photocatalysts for water splitting and pollutant degradation over the past few decades [7, 8], their efficiency toward organic synthesis is relatively low because of the poor yield and selectivity in the generation of reactive intermediate radicals. In addition, the toxic heavy metal content and photocorrosive character of metal-containing photocatalysts further restrict their practical application [9]. Bearing this in mind, metal-free species with suitable band structures for promising ROS generation would be ideal catalysts for light-driven organic synthesis. Recently, metal-free materials such as graphene oxide and graphitic-carbon nitride have been proposed as photocatalysts for organic synthesis, such as for the selective aerobic oxidation of amines, selective oxidation of sulfides, and so on [10–12]. However, due to the lack of suitable band structures for long wavelength absorption, their catalytic activities are still insufficient, especially considering that the visible light region accounts for almost 44% of the total energy from sunlight.

As a novel kind of metal-free photocatalysts, conjugated polymer-based semiconductors have attracted wide attention because of their unique electronic structure, extraordinary chemical/physical stability, and high conductivity [13–18]. Furthermore, owing to the various possible molecular designs, conjugated polymers possess tunable band structures with wide range light absorption. However, only a few conjugated polymers, such as poly(diphenylbutadiyne) [16] and poly(3,4-ethylenedioxythiophene) [17], have been established as photocatalysts under visible light irradiation, which motivated us to prepare more active conjugated polymers with enriched electronic structures. Therefore, we envisioned that appropriate monomers with electron rich atoms, such as sulfur, oxygen, and fluorine, would be beneficial for the design of conjugated structure-based polymers with optimized catalytic activity.

More importantly, we anticipated that the band structure of certain conjugated polymers could be systematically controlled by modulating their molecular chain length. As an example, we first focused on 3-hexylthiophene, which contains a five-membered aromatic ring consisting of four carbon atoms and one sulfur [19–22]. In 3-hexylthiophene, the lone electron pair on the sulfur atom is delocalized over the π-electron system forming an electron-rich π-conjugated structure [23]. Further, theoretical calculations via density functional theory (DFT) revealed that the band structure of poly(3-hexylthiophene) (PHT) is closely related to the number of monomeric units (n), whose highest occupied molecular orbital/lowest unoccupied molecular orbital (HOMO/LUMO) levels, as well as the corresponding electron clouds, are presented in Fig. 1. As seen, the bandgap for the 3-hexylthiophene monomer (n = 1) was estimated to be ~ 5.98 eV, too large to be suitable for photocatalytic
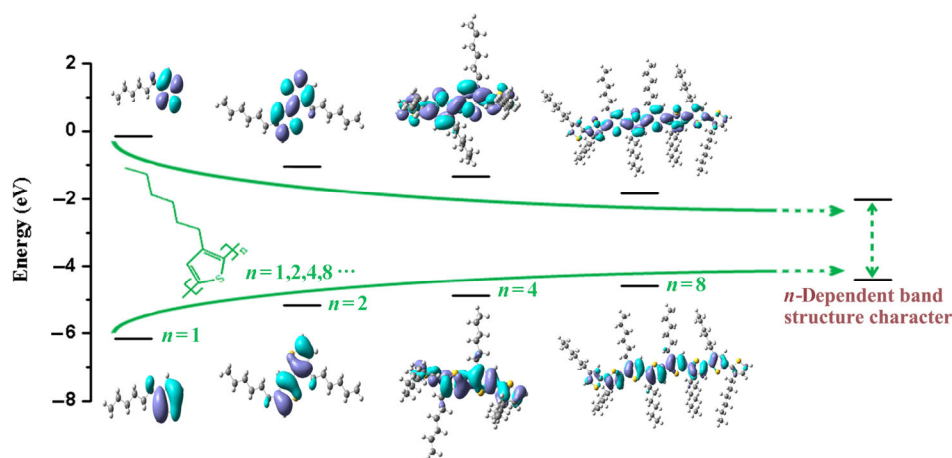
Figure 1 Molecular orbital diagram of the evaluated HOMO and LUMO levels of PHT at different values of n. Here, n denotes the number of monomeric units in poly(3-hexylthiophene).

applications. It is interesting that the bandgap of PHT is strongly related to the number of monomeric units; the larger the n is, the narrower the bandgap becomes. For example, the calculated bandgap of PHT decreased to 4.13 eV at $n = 2$. Further, the HOMO and LUMO levels got closer when the number of monomeric units in PHT increased to 4 and 8, with bandgaps of 3.56 and 2.77 eV, respectively. The above results clearly demonstrate that the PHT bandgap can be easily controlled through structural design, and that PHT may become visible-light responsive ($E \leq 2.91$ eV) by controlling the number of monomeric units.

2 Experimental

2.1 Synthesis of PHT

PHT was synthesized by the typical catalyst-transfer Kumada polycondensation reaction. 2-Bromo-5-iodo-3-hexylthiophene (1.75 g, 4.7 mmol) was dissolved in THF (50 mL) in a three-neck flask and stirred under N_2. After the solution was cooled to 0 °C, 2.35 mL THF with 4.7 mmol of isopropylmagnesium chloride (i-PrMgCl) was added with a syringe and the mixture was stirred for 30 min. The reaction solution was then heated to 35 °C and 0.0675 g (0.124 mmol) of (1,3-bis(diphenylphosphino)-propane)-dichloronickel (II) (Ni(dppp)Cl$_2$) was added, followed by stirring for 2 h. 5 mL HCl solution (50 wt.%) was added to quench the above reaction, and a deep red solid was recrystallized after removing the solvent of methanol and hexane under vacuum. The solid was recrystallized from methanol and hexane. The monomer 2-bromo-5-iodo-3-hexylthiophene was synthesized according to Ref. [24]. The resulting PHT polymer presented a molecular weight (M_W) of 9,700 with a polymer dispersity index (PDI) of 1.14. ^{1}H NMR (500 MHz, CDCl$_3$, δ (ppm)): 6.98 (s, 1H), 2.80 (t, 2H), 1.71 (m, 2H), 1.34 (m, 2H), 0.91 (t, 3H).

2.2 General procedure for the self-coupling of benzylamine and its derivatives

A sealed vial containing an amine (5 µL), the PHT nanofiber photocatalyst (5 mg), and 2 mL CH$_3$CN was purged with oxygen/argon/air, and placed in a water bath under visible light irradiation ($\lambda \geq 450$ nm) for 4 h.

When the reaction was completed, the photocatalyst was removed by centrifugation. The conversion and selectivity were determined by ^{1}H NMR spectroscopy using CDCl$_3$ as the solvent and terephthalonitrile as the internal standard reference.

2.3 Photodegradation of methylene blue

The photodegradation reaction of methylene blue (MB) was carried out in a quartz container using a xenon lamp (PLSSXE300/300UV, Trusttech Co., Ltd. Beijing) as the sunlight source or a visible light source with a 450 nm long pass filter. Before irradiation, PHT nanofibers, g-C$_3$N$_4$, and P25-TiO$_2$ (2 mg·mL^{-1}) were stirred in an MB solution (4 mg·mL^{-1}) in the dark for 1 h to reach the adsorption/desorption equilibrium. Samples were taken at different times, followed by centrifugation to separate the catalysts (particularly for g-C$_3$N$_4$ and P25-TiO$_2$) and obtain transparent solutions. Then, the MB solutions were characterized on a Lambda 950 UV-vis spectrophotometer, and the intensity of the signal with maximum absorption at 674 nm was monitored. After completion of the MB degradation, the PHT nanofibers were recovered by centrifugation and washed thoroughly with deionized water. The dried PHT nanofibers were re-used in subsequent cycles under identical conditions.

2.4 Detection of hydroxyl radicals

The quantitative analysis of ·OH radical formation under visible light irradiation was performed by the photoluminescence (PL) technique employing terephthalic acid (TPA) as the probe, which readily reacts with ·OH radicals to produce a highly fluorescent product, 2-hydroxyterephthalic acid (HTPA). A mixed aqueous solution (200 mL) consisting of TPA (50 mg, 0.3 mmol) and sodium hydroxide (40 mg, 1 mmol) was firstly prepared under magnetic stirring, followed by addition of 100 mg PHT nanofibers as the catalyst. Under different gas atmospheres (argon, oxygen, and air), the solutions were irradiated with visible light ($\lambda \geq 450$ nm) for 70 min at room temperature. Aliquots of 3 mL were taken from the reaction mixture at time intervals of 10 min, centrifuged, and analyzed by photoluminescence spectroscopy (λ_{ex} = 315 nm, slitex corresponding to a band-pass of 5.0 nm, slitem corresponding to a band-pass of 10.0 nm). The for-

mation of HTPA was monitored by the emission band of the corresponding anion at 426 nm. The hydroxylation reaction of TPA proceeds typically through ·OH radicals at low concentrations ($\leq 10^{-3}$ M) [25].

2.5 Theoretical calculations

The optimization was carried out with the B3LYP (6–31 G(d)) functional with Cs symmetry constraints. Then, time-dependent density functional theory (TDDFT) calculations were performed on the optimized structures. All the calculations, including optimizations and TDDFT, were conducted with the G03 software. Geometry optimization and TDDFT calculations were performed with the basis set 6–31G for carbon, hydrogen, and sulfur atoms.

2.6 Sample characterization

Field emission scanning electron microscopy (FESEM, Ultra 55, Zeiss) characterization was carried out at an acceleration voltage of 5 kV. Transmission electron microscopy (TEM) images were obtained on a JEM-2100F field emission electron microscope at an acceleration voltage of 200 kV. Fourier transform infrared (FTIR) measurements were carried out on a Magna-IR750 FTIR spectrometer on KBr pellets at room temperature. Room-temperature UV-vis absorption spectra were recorded on a Lambda 950 UV-vis spectrophotometer using 0.2 g·L^{-1} PHT nanofibers in a trichloromethane solution. Gel permeation chromatography (GPC) was carried out at 35 °C using an Agilent 1100 system equipped with both G1362A refractive-index and G1314A UV detectors (eluent: THF; calibration: Polystyrene standard). X-ray diffraction (XRD) experiments were performed on a PANalytical X'Pert PRO X-ray diffractometer using Cu Kα radiation (λ = 1.542 Å) operating at 40 kV and 40 mA from 2θ = 2.5°–25°. Thermogravimetric (TG) analysis (Pyris 1 TGA, PerkinElmer) was performed under N$_2$ atmosphere from 100 to 750 °C at a heating rate of 5 °C·min^{-1}. ^{1}H nuclear magnetic resonance (NMR) spectra were recorded on an AVANCE III HD 400 MHz spectrometer in CDCl$_3$. Electron spin resonance (ESR) measurements were performed using a Bruker EMX plus model spectrometer operating at X-band frequencies (9.4 GHz) at room temperature.

2.7 Electrochemical tests

Mott–Schottky tests were carried out on an electrochemical station (CHI660B, Shanghai Chenhua Limited, China) under ambient conditions with a conventional three-electrode cell in 1.0 M Na$_2$SO$_4$ solution. In detail, a grounded glassy carbon electrode, on which each sample was deposited, was employed as the working electrode, while Pt wire and standard Ag/AgCl (3 M KCl) electrodes were used as the counter and reference electrodes, respectively. The electrode was prepared by dropping 10 µL of a PHT nanofiber solution (1 g·L^{-1}, trichloromethane) on a grounded glassy carbon electrode. After drying in air, Mott–Schottky tests were performed at potentials ranging from –0.1 to 0.1 V (vs. Ag/AgCl) at selected frequencies of 10, 20, and 30 kHz in 1.0 M Na$_2$SO$_4$ solution.

3 Results and discussion

In this study, conjugated polymer nanofibers of PHT were obtained by the catalyst-transfer Kumada polycondensation strategy depicted in Fig. 2(a) (see details in the Electronic Supplementary Material (ESM)). After polymerization in THF solution, the pale yellow-colored 3-hexylthiophene monomer turned into the orange PHT polymer (Fig. 2(b)). The molecular chain structure and crystallization behavior of the as-synthesized PHT were investigated by NMR spectroscopy and XRD. The ^{1}H NMR spectrum in Fig. S1 in the ESM shows the high regioregularity of PHT with ~ 99% head-to-tail coupling as indicated by the signal with chemical shift (δ) 6.98 ppm [24]. As shown in Fig. S2 in the ESM, the strong diffraction peaks are readily indexed to the (100), (200), and (300) planes of PHT, indicating its high crystallinity. The successful synthesis of PHT was further confirmed by FTIR spectroscopy (Fig. 2(c)), showing absorption bands for the C–H stretching vibration of hexyl groups at 2,956, 2,925, and 2,855 cm^{-1}, and a band for the symmetric C=C stretching mode of thiophene rings located at 1,459 cm^{-1}. The morphology of PHT was studied by TEM, from which nanofibers with uniform diameter of ~ 20 nm and length up to a few micrometers were observed (Fig. 2(d)). Experimentally, the average value of n was determined through the degree
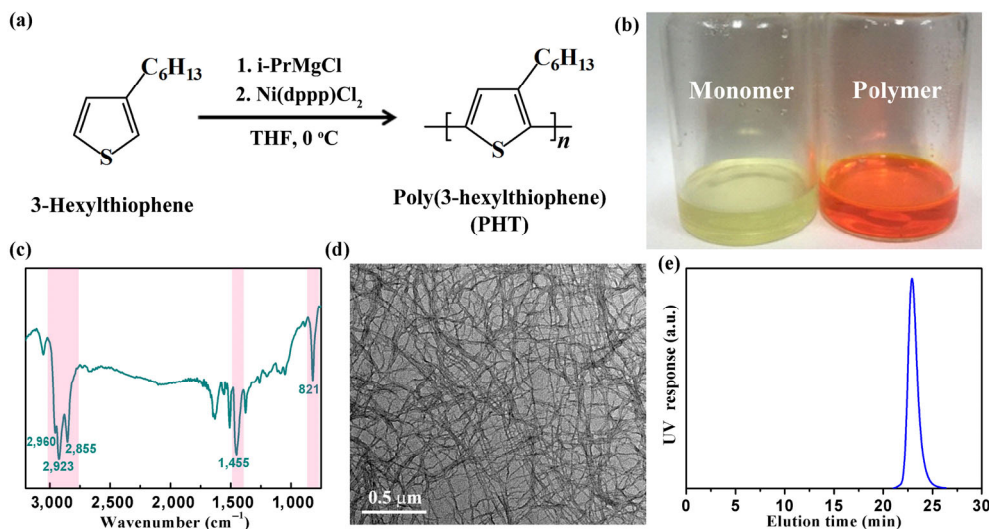
Figure 2 (a) Schematic illustration of the polymerization process for PHT. (b) Photograph of 3-hexylthiophene (pale yellow) and PHT (orange) compounds in tetrahydrofuran solution. (c) FTIR spectrum of PHT. (d) TEM image of PHT. (e) Gel permeation chromatography trace of PHT.

of polymerization (DP) using the GPC method. As shown in Fig. 2(e), the monomodal peak proves a narrow molecular weight distribution of PHT with a polydispersity index of 1.14. The obtained molecular weight of 9,700 g·mol^{-1} for PHT indicates its DP to be approximately 57.

According to the theoretical studies, PHT nanofibers

with DP of about 57 would possess a suitable bandgap for visible light photoresponse. In order to provide insight on the role the DP has on the band structure of the conjugated polymer, the light absorption properties of PHT were investigated. As shown in the UV-vis absorption spectrum in Fig. 3(a), the PHT nanofibers exhibit a single absorption peak located
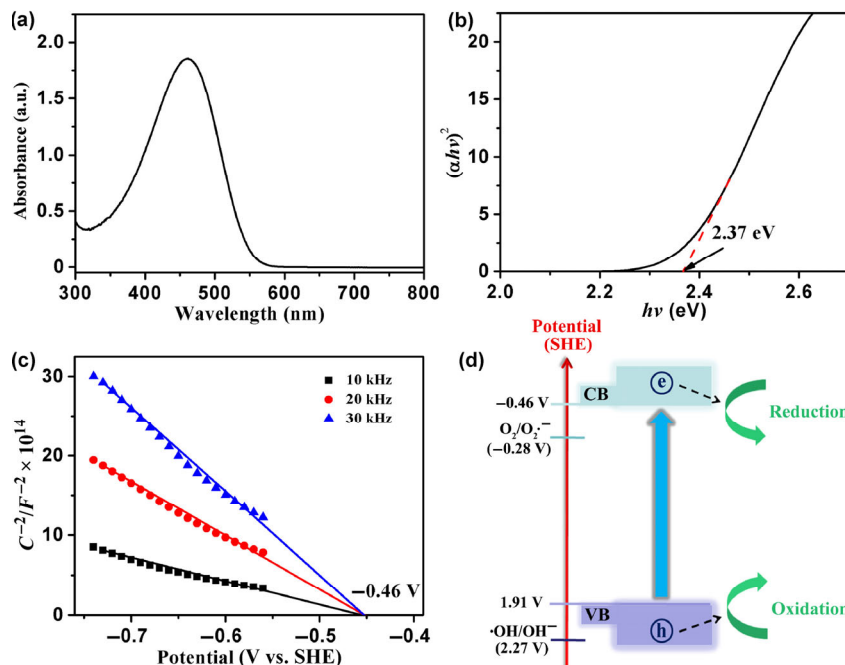

Figure 3 (a) UV-vis absorption spectrum and (b) the corresponding bandgap of the PHT nanofibers. (c) Mott–Schottky plots of PHT nanofibers with a flat band potential vs. SHE. (d) Valence band and conduction band of PHT nanofibers; the redox potential for the conversion of oxygen molecules into superoxide ions and that of OH^{-} into hydroxyl radicals are also shown.

at 460 nm, corresponding to a bandgap of 2.37 eV (Fig. 3(b)), revealing their potential visible light-responsive properties. The band structure of the PHT nanofibers was further studied by a Mott–Schottky plot analysis (Fig. 3(c)), showing a flat band potential vs. the standard hydrogen electrode (SHE) of –0.46 V. Consequently, based on the above results, the valence band (VB) of the PHT nanofibers was calculated to be 1.91 V vs. SHE. Therefore, the synthesized PHT nanofibers with a bandgap of 2.37 eV are a promising photocatalyst for visible light photocatalysis, as illustrated in Fig. 3(d).

Herein, the photocatalytic activity of the PHT nanofibers was firstly evaluated toward the degradation of MB under visible light irradiation ($\lambda \geq 450$ nm). As shown in Fig. 4(a), the synthetic PHT nanofibers
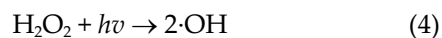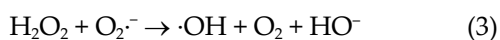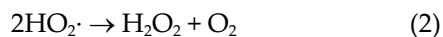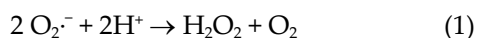
exhibited excellent photocatalytic activity and fully degraded the MB dye within 75 min, much faster than the degradation with graphitic-carbon nitride (g-C_3N_4) [26] and P25-TiO_2 powders. Additionally, the photocatalytic activity of PHT nanofibers was found to be very stable, with negligible variation even after five cycles (Fig. 4(b)).

As previously reported [3, 16], the photodegradation of organic dyes with semiconductors is strongly related to the generation of reactive oxygen species such as ·OH, $O_2{\cdot}^-$, and/or $^1O_2$. Therefore, in this study, it was crucial to identify what ROS were generated by the PHT nanofibers causing the observed dye degradation under visible light irradiation. As the most direct evidence for the identification of the generated ROS, ESR measurements were performed on the PHT
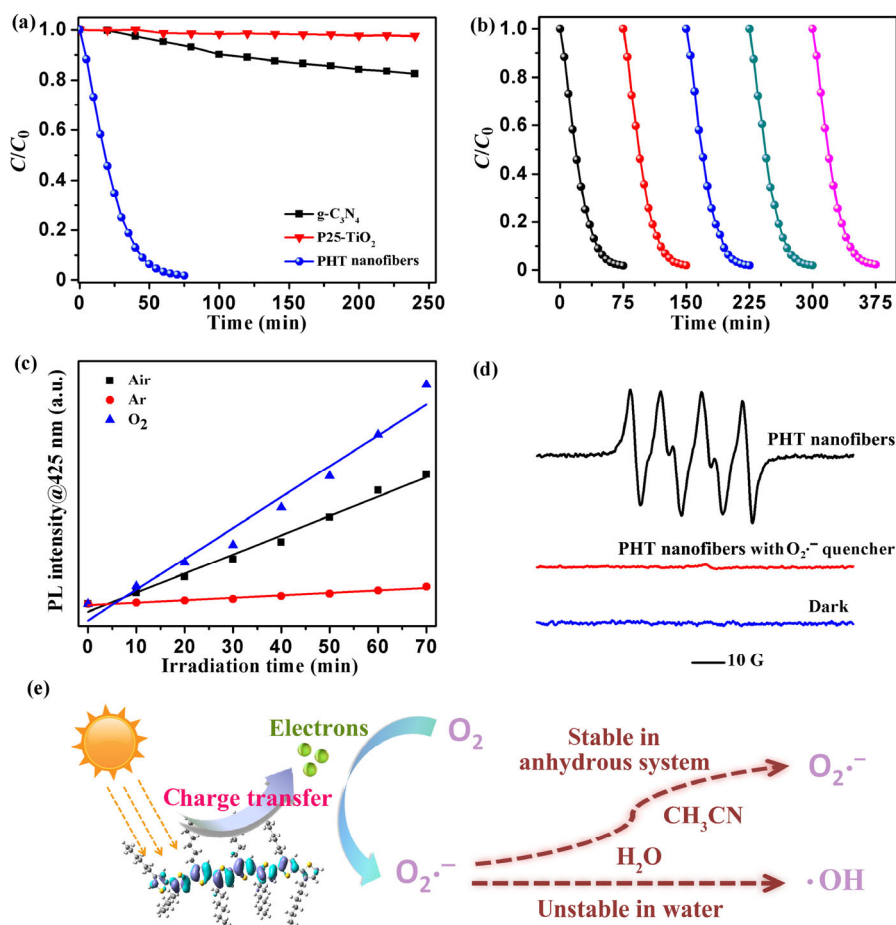
Figure 4 (a) Photocatalytic degradation of MB in the presence of PHT nanofibers, g-C_3N_4, and P25-TiO_2 under visible light ($\lambda \geq 450$ nm) irradiation. (b) Cycling stability of PHT nanofibers for MB degradation under visible light irradiation. (c) Plots of the PL intensity at 426 nm against the irradiation time; the fluorescence spectra were recorded every 10 min under visible light illumination. (d) ESR spectra of PHT nanofibers in the presence of DMPO in acetonitrile solution under different conditions. (e) Schematic of the solvent-dependent generation of various oxygen radicals by PHT nanofibers under visible light irradiation.

nanofibers. 2,2,6,6-Tetramethylpiperidine (TEMP) and 5,5-dimethyl-1-pyrroline-N-oxide (DMPO) were selected as trapping agents for $^1O_2$ and $O_2^{\cdot-}$/$\cdot$OH, respectively. As shown in Fig. S9 in the ESM, no obvious signal could be detected with TEMP in neither aqueous nor acetonitrile solutions, indicating that no $^1O_2$ was generated in this system. Subsequently, further ESR tests were carried out using DMPO as the trapping agent to examine the possible generation of $O_2^{\cdot-}$ or $\cdot$OH by the PHT nanofibers. As seen from Fig. S10 in the ESM, the ESR spectrum of the PHT nanofibers displays the 1:2:2:1 quartet characteristic of the formation of DMPO–OH, indicating the presence of $\cdot$OH radicals in the system. However, according to the band structure of PHT nanofibers with a VB energy level of 1.91 V vs. SHE shown in Fig. 3(d), it is unlikely that hydroxyl radicals are produced from the oxidation of OH$^-$ by the photogenerated holes of PHT. On the basis that the generation of $\cdot$OH is not dependent on the atmosphere used while that of $O_2^{\cdot-}$ is oxygen-dependent, we further studied the possible generation of $\cdot$OH under various atmospheres using TPA as the indicator, which can selectively react with $\cdot$OH to form 2-hydroxyterephthalic exhibiting fluorescence at 426 nm. As seen in Fig. 4(c), the generation of $\cdot$OH was almost inhibited under Ar and greatly enhanced under O_2, indicating an oxygen content-dependent character. This phenomenon clearly indicates that the generated ROS by PHT nanofibers is not $\cdot$OH but $O_2^{\cdot-}$. Based on the above results, a major question arises: Why is only the signal of $\cdot$OH detected, instead of the $O_2^{\cdot-}$ one more suited for the band structure of PHT nanofibers? It must be noted that $O_2^{\cdot-}$ is not stable in water, and can be transformed into $\cdot$OH through the following possible reactions [16, 17]
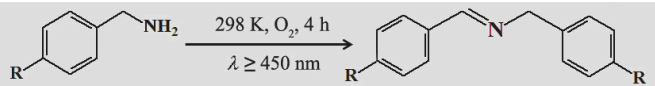
$$2\,O_2^{\cdot-} + 2H^+ \rightarrow H_2O_2 + O_2 \tag{1}$$

$$2HO_2\cdot \rightarrow H_2O_2 + O_2 \tag{2}$$

$$H_2O_2 + O_2^{\cdot-} \rightarrow \cdot OH + O_2 + HO^- \tag{3}$$

$$H_2O_2 + h\nu \rightarrow 2\cdot OH \tag{4}$$

In order to reasonably examine the possible transformation of $O_2^{\cdot-}$ into $\cdot$OH, ESR tests on PHT nanofibers in acetonitrile solution were carried out so as to exclude the influence of H_2O on the generated ROS. The new ESR spectrum displays a single quartet

with relative intensities of 1:1:1:1, assigned to $O_2^{\cdot-}$. In addition, the ESR signal could be inhibited by addition of benzoquinone, a distinctive quencher for superoxide, further confirming the generation of $O_2^{\cdot-}$ by PHT (Fig. 4(d)). In that case, we propose that $O_2^{\cdot-}$ is firstly generated via molecule oxygen activation by the PHT nanofibers, which rapidly reacts with H_2O molecules and is converted into $\cdot$OH, leading to the absence of the $O_2^{\cdot-}$ signal in the ESR spectrum (Fig. 4(e)). The above results clearly indicate that the generated ROS by PHT nanofibers is $O_2^{\cdot-}$ and not $\cdot$OH.

On the basis of their high selectivity and efficiency for $O_2^{\cdot-}$ generation, the PHT nanofibers were expected to be an excellent photocatalyst for selective oxidation reactions. Herein, the selective aerobic oxidation of amines to imines, an essential reaction for the preparation of chemical intermediates, was selected to investigate the catalytic activity of PHT nanofibers. As shown in Fig. S12 in the ESM, the chemoselectivity toward such organic synthesis reaction was nearly 100% at different irradiation times, while the yield of N-benzylidene benzylamine was closely related to the reaction time, indicating its time-dependent character. In comparison, although the PHT nanofibers were able to oxidize benzylamine in air, its conversion toward the imine was very low (only ~ 35%). Even worse, PHT nanofibers exhibited a negligible photo-catalytic effect toward benzylamine under inert atmosphere with a negligible conversion rate of ~ 5%, revealing the oxygen-dependent character (Table 1, entries 2–4) and crucial role of $O_2^{\cdot-}$ generation for this self-coupling reaction. Notably, high selectivities were obtained in general regardless of the atmosphere used, which further demonstrates the purity of the generated oxygen radicals.

To further prove the key role of $O_2^{\cdot-}$ in the above photocatalytic organic transformations, benzoquinone, a superoxide quencher, was added to one of the vials and was found to successfully inhibit the photocatalytic reaction, while negligible influence was observed after adding a hydroxyl radical quencher (Table 1, entries 5 and 6). More importantly, PHT nanofibers were found to also be a universal catalyst for other organic syntheses. A series of benzylamine derivatives with different substituent groups were further chosen

Table 1 Self-coupling of various amines to imines catalyzed by PHT nanofibers

Entry[a]	Catalyst	R	Atmosphere	Additive	Conversion (%)	Selectivity (%)
1	–	H	O_2	–	0	0
2	PHT	H	O_2	–	99	99
3	PHT	H	Ar	–	5	99
4	PHT	H	Air	–	35	99
5	PHT	H	O_2	·OH quencher	99	98
6	PHT	H	O_2	$O_2^{·-}$ quencher	16	97
7	PHT	Cl	O_2	–	98	97
8	PHT	F	O_2	–	98	98
9	PHT	CH_3	O_2	–	98	97
10	PHT	OCH_3	O_2	–	94	97

[a] Reaction conditions: Amine (5 μL), PHT nanofibers (10 mg), 2 mL CH_3CN, 4 h, water bath, room temperature (298 K), under visible light irradiation ($\lambda \geq 450$ nm). The conversion and selectivity were determined by ^1H NMR spectroscopy. The used hydroxyl radical and superoxide quenchers were mannitol and benzoquinone, respectively.

to evaluate the catalytic activity of the PHT nanofibers (Table 1, entries 7–10). It was found that the PHT nanofibers afforded a nearly complete conversion of amines into the corresponding imines in the presence of either electron-withdrawing substituent groups (Cl, entry 7; F, entry 8) or electron-donating substituent groups (CH_3, entry 9; OCH_3, entry 10). Furthermore, the photocatalytic activity of PHT nanofibers was highly stable even after a number of reaction cycles (Table S1 in the ESM). As shown in Fig. S14 in the ESM, the PHT nanofibers maintained their original chemical structure after the cycling tests, demonstrating their photostability for potential practical applications. Additionally, the mechanism for the self-coupling reaction of PHT nanofibers was investigated. As illustrated in Fig. S15 in the ESM, electron (e^-) and hole (h^+) pairs are initially photogenerated on the surface of the PHT nanofibers under visible light irradiation. After losing an electron to a photogenerated hole of a PHT nanofiber, a benzylamine molecule is converted into a carbocationic radical-type intermediate, which possesses high activity toward $O_2^{·-}$ to generate an intermediate hydroperoxy (phenyl)methanamine. After further elimination of NH_2OH/H_2O_2 and H_2O/NH_3 molecules, the coupled product N-benzylidene benzylamine is obtained [14, 27].

4 Conclusions

In conclusion, we have proposed a strategy to prepare conjugated polymer-based photocatalysts with suitable band structures via molecular design. As an example, for the first time, we show that PHT nanofibers with a degree of polymerization of ~ 57 are an efficient photocatalyst for organic synthesis under visible light irradiation. PHT nanofibers with a uniform diameter of ~ 20 nm and length up to a few micrometers were successfully synthesized by catalyst-transfer Kumada polycondensation. Both theoretical calculation and experimental data indicate that the PHT nanofibers are visible light-driven catalysts with a suitable bandgap of ~ 2.37 eV. Hence, the PHT nanofibers were able to self-couple a range of amines into imines with nearly 100% conversion and selectivity, owing to the selective transformation of molecular oxygen into superoxide ions. Furthermore, the PHT nanofibers exhibited superior stability without structural degradation after several photocatalytic cycles, demonstrating their practical application value. We believe that this study not only extends the applications of PHTs into the photocatalysis field, but also provides new insight for the design of conjugated polymer-based photocatalysts.

Acknowledgements

Electronic Supplementary Material: Supplementary material is available in the online version of this article at https://doi.org/10.1007/s12274-017-1729-6.

References

[1] Yoon, T. P.; Ischay, M. A.; Du, N. Visible light photocatalysis as a greener approach to photochemical synthesis. *Nat. Chem.* **2010**, *2*, 527–532.

[2] Hisatomi, T.; Kubota, J.; Domen, K. Recent advances in semiconductors for photocatalytic and photoelectrochemical water splitting. *Chem. Soc. Rev.* **2014**, *43*, 7520–7535.

[3] Chen, X. B.; Liu, L.; Yu, P. Y.; Mao, S. S. Increasing solar absorption for photocatalysis with black hydrogenated titanium dioxide nanocrystals. *Science* **2011**, *331*, 746–750.

[4] Yang, X. J.; Xu, X. M.; Xu, J.; Han, Y. F. Iron oxychloride (FeOCl): An efficient Fenton-like catalyst for producing hydroxyl radicals in degradation of organic contaminants. *J. Am. Chem. Soc.* **2013**, *135*, 16058–16061.

[5] Apel, K.; Hirt, K. Reactive oxygen species: Metabolism, oxidative stress, and signal transduction. *Annu. Rev. Plant Biol.* **2004**, *55*, 373–399.

[6] Wang, H.; Yang, X. Z.; Shao, W.; Chen, S. C.; Xie, J. F.; Zhang, X. D.; Wang, J.; Xie, Y. Ultrathin black phosphorus nanosheets for efficient singlet oxygen generation. *J. Am. Chem. Soc.* **2015**, *137*, 11376–11382.

[7] Prier, C. K.; Rankic, D. A.; MacMillan, D. W. C. Visible light photoredox catalysis with transition metal complexes: Applications in organic synthesis. *Chem. Rev.* **2013**, *113*, 5322–5363.

[8] Han, C.; Chen, Z.; Zhang, N.; Colmenares, J. C.; Xu, Y. J. Hierarchically CdS decorated 1D ZnO nanorods-2D graphene hybrids: Low temperature synthesis and enhanced photocatalytic performance. *Adv. Funct. Mater.* **2015**, *25*, 221–229.

[9] Martin, D. J.; Liu, G. G.; Moniz, S. J. A.; Bi, Y. P.; Beale, A. M.; Ye, J. H.; Tang, J. W. Efficient visible driven photocatalyst, silver phosphate: Performance, understanding

and perspective. *Chem. Soc. Rev.* **2015**, *44*, 7808–7828.

[10] Zhang, N.; Zhang, Y. H.; Xu, Y. J. Recent progress on graphene-based photocatalysts: Current status and future perspectives. *Nanoscale* **2012**, *4*, 5792–5813.

[11] Wang, Y.; Wang, X. C.; Antonietti, M. Polymeric graphitic carbon nitride as a heterogeneous organocatalyst: From photochemistry to multipurpose catalysis to sustainable chemistry. *Angew. Chem., Int. Ed.* **2012**, *51*, 68–89.

[12] Su, F. Z.; Mathew, S. C.; Lipner, G.; Fu, X. Z.; Antonietti, M.; Blechert, S.; Wang, X. C. mpg-C_3N_4-catalyzed selective oxidation of alcohols using O_2 and visible light. *J. Am. Chem. Soc.* **2010**, *132*, 16299–16301.

[13] Heinze, J.; Frontana-Uribe, B. A.; Ludwigs, S. Electrochemistry of conducting polymers-persistent models and new concepts. *Chem. Rev.* **2010**, *110*, 4724–4771.

[14] Wang, Z. J.; Ghasimi, S.; Landfester, K.; Zhang, K. A. I. Molecular structural design of conjugated microporous poly(benzooxadiazole) networks for enhanced photocatalytic activity with visible light. *Adv. Mater.* **2015**, *27*, 6265–6270.

[15] Zhou, Q. Q.; Shi, G. Q. Conducting polymer-based catalysts. *J. Am. Chem. Soc.* **2016**, *138*, 2868–2876.

[16] Ghosh, S.; Kouamé, N. A.; Ramos, L.; Remita, S.; Dazzi, A.; Deniset-Besseau, A.; Beaunier, P.; Goubard, F.; Aubert, P. H.; Remita, H. Conducting polymer nanostructures for photocatalysis under visible light. *Nat. Mater.* **2015**, *14*, 505–511.

[17] Ghosh, S.; Kouame, N. A.; Remita, S.; Ramos, L.; Goubard, F.; Aubert, P. H.; Dazzi, A.; Deniset-Besseau, A.; Remita, H. Visible-light active conducting polymer nanostructures with superior photocatalytic activity. *Sci. Rep.* **2015**, *5*, 18002.

[18] Chen, Y.; Zhang, J. S.; Zhang, M. W.; Wang, X. C. Molecular and textural engineering of conjugated carbon nitride catalysts for selective oxidation of alcohols with visible light. *Chem. Sci.* **2013**, *4*, 3244–3248.

[19] Osaka, I.; McCullough, R. D. Advances in molecular design and synthesis of regioregular polythiophenes. *Acc. Chem. Res.* **2008**, *41*, 1202–1214.

[20] Dudenko, D.; Kiersnowski, A.; Shu, J.; Pisula, W.; Sebastiani, D.; Spiess, H. W.; Hansen, M. R. A strategy for revealing the packing in semicrystalline π-conjugated polymers: Crystal structure of bulk poly-3-hexyl-thiophene (P3HT). *Angew. Chem., Int. Ed.* **2012**, *51*, 11068–11072.

[21] Khanduyeva, N.; Senkovskyy, V.; Beryozkina, T.; Horecha, M.; Stamm, M.; Uhrich, C.; Riede, M.; Leo, K.; Kiriy, A. Surface engineering using Kumada catalyst-transfer polycondensation (KCTP): Preparation and structuring of poly(3-hexylthiophene)-based graft copolymer brushes. *J. Am. Chem. Soc.* **2009**, *131*, 153–161.

[22] Nielsen, C. B.; McCulloch, I. Recent advances in transistor performance of polythiophenes. *Prog. Polym. Sci.* **2013**, *38*, 2053–2069.

[23] Sulzbach, H. M.; Schleter, P. V. R.; Jiao, H. J.; Xie, Y. M.; Schaefer, H. F. A [10]annulene isomer may be aromatic, after all! *J. Am. Chem. Soc.* **1995**, *117*, 1369–1373.

[24] McCullough, R. D. The chemistry of conducting polythiophenes. *Adv. Mater.* **1998**, *10*, 93–116.

[25] Ishibashi, K.; Fujishima, A.; Watanabe, T.; Hashimoto, K. Detection of active oxidative species in TiO_2 photocatalysis

using the fluorescence technique. *Electrochem. Commun.* **2000**, *2*, 207–210.

[26] Bojdys, M. J.; Müller, J. O.; Antonietti, M.; Thomas, A. Ionothermal synthesis of crystalline, condensed, graphitic carbon nitride. *Chem.—Eur. J.* **2008**, *14*, 8177–8182.

[27] Riente, P.; Adams, A. M.; Albero, J.; Palomares, E.; Pericàs, M. A. Light-driven organocatalysis using inexpensive, nontoxic Bi_2O_3 as the photocatalyst. *Angew. Chem., Int. Ed.* **2014**, *53*, 9613–9616.